Intermediate ground states of hydrogen in $LaNiO_2$: A first-principles study

Xiangru Han,[1] Pei Li,[1] Xuelei Sui,[2,1,*] Heng Jin,[3,1] Feng Luo,[4,5] Liang Qiao,[5] and Bing Huang[1,3,†]

[1]*Beijing Computational Science Research Center, Beijing, China*
[2]*College of Mathematics and Physics, Beijing University of Chemical Technology, Beijing 100029, China*
[3]*Department of Physics, Beijing Normal University, Beijing 100875, China*
[4]*School of Mechanical Engineering, Chengdu University, Chengdu 610106, China*
[5]*School of Physics, University of Electronic Science and Technology of China, Chengdu 610106, China*

(Received 8 June 2023; revised 22 September 2023; accepted 9 October 2023; published 24 October 2023)

Infinite-layer nickelate superconductors RNiO$_2$ (R = La, Nd, Pr) are synthesized via chemical reduction using the CaH_2 agent, and the unintentional introduction of H dopant during the reduction process may affect RNiO$_2$ quality and ultimately determine their electronic properties. However, the ground-state configurations and electronic structures of RNiO$_2$ under varying H concentrations (δ) remain unclear. In this work, we employ the cluster-expansion method and first-principles calculations to examine the intermediate ground-state structures, electronic structures, and magnetic properties of $LaNiO_2H_\delta$ ($0 < \delta < 1$). Interestingly, our results show that H always occupies apical oxygen vacancies, forming ordered H-Ni-H chains along the out-of-plane direction but with different δ-dependent patterns along the in-plane direction. Notably, the interstitial s-like orbital in the $LaNiO_2$ host is annihilated by H and the filling of the Ni $3d$ bands, especially the $3d_{x^2-y^2}$ and $3d_{z^2}$ orbitals, is greatly altered. With H doping, both enhanced magnetic stability of G-type antiferromagnetic states and simultaneous metal-to-insulator transition occur. Our study demonstrates the remarkable doping impact of H in $LaNiO_2$, allowing us to gain deeper insight into the structure and superconductivity of infinite-layer nickelates.

DOI: 10.1103/PhysRevB.108.165145

I. INTRODUCTION

The infinite-layer nickelate superconductors represent new platforms for the study of unconventional superconductivity. Observed in $NdNiO_2$ [1–3], unconventional superconducting behaviors have also been observed in $PrNiO_2$ [4,5], $LaNiO_2$ [6], etc. [7]. This leads to comprehensive studies in nickelate superconductors RNiO$_2$ (R = La, Nd, Pr) [8–24]. Furthermore, a successive detection of magnetic fluctuations [25,26] and charge density waves [27,28] within the nickelate family has raised the intriguing question regarding their similarity to cuprates. However, due to challenges in reduction synthesis by CaH_2 agents, only a few groups worldwide have reproduced superconducting behaviors in nickelates [1,29]. Very recently, Ding *et al.* demonstrated that unintentional H doping may commonly present in epitaxial infinite-layer nickelates. Furthermore, they found that the insertion of H atoms may modulate orbital hybridization, thereby exerting control over the overall superconducting phase diagram of the samples [30].

Theoretical studies of RNiO$_2$ indicate that H atoms have noticeable influences on the Fermi surfaces, electronic correlations, and magnetic stability of these systems [30–32]. However, these studies are all based on several artificial H concentrations (δ) in $P4/mmm$ supercells [30–32]. Thus, it is doubtful whether the conclusions obtained from these artificial structures are reliable. In a real doped system, homogeneous intermediate ground states can exist for specific δ, while at any arbitrary δ inhomogeneous phases may also exist in between these intermediate ground states [33,34]. To obtain a comprehensive understanding of the physical properties of a doped system, it is necessary to investigate numerous atomic configurations to identify the possible intermediate ground states. However, it should be noted that such extensive research on RNiO$_2$ is currently lacking.

To determine the multiple intermediate configurations in RNiO$_2$H$_\delta$ ($0 < \delta < 1$), the cluster expansion (CE) method, commonly adopted in binary alloys [35–37], can be used to search for the intermediate ground states in our study, considering "vacancy" and H atom as two kinds of alloying atoms. With possible intermediate ground states of infinite-layer nickelates, we may yield a deeper understanding of superconductivity in RNiO$_2$H$_\delta$ by examining the relationship between H doping and the electronic properties of RNiO$_2$.

In this study, a combination of the CE method and first-principles calculations has been performed to obtain intermediate configurations. In addition to $LaNiO_2$ and $LaNiO_2H$, four intermediate ground states with different δ (δ = 0.33, 0.5, 0.67, 0.83) are found in $LaNiO_2H_\delta$. Interestingly, there are two basic rules for the stable configurations of H in $LaNiO_2H_\delta$, that is, (i) H atoms occupy the apical oxygen vacancies, forming ordered H-Ni-H chains along the out-of-plane direction, and (ii) H can exhibit different δ-dependent ordered in-plane patterns. As for electronic structure, the insertion of H results in two distinct local environments of Ni (NiO_4 and NiO_4H_2) and significantly alters the orbital

*xueleisui@buct.edu.cn
†bing.huang@csrc.ac.cn

 ©2023 American Physical Society

fillings of Ni 3*d* orbitals. Consequently, it modulates the orbital polarization that is related to the superconductivity in $LaNiO_2H_\delta$. Importantly, in the *G*-type antiferromagnetic (AFM-*G*) states which exhibit the lowest energy, the spin-polarization energy increases with δ, accompanied by an unexpected metal-to-insulator transition. Our study provides insight into the structural and electronic structure properties of nickelates, specifically focusing on the effects of more realistic H doping conditions.

II. METHOD

The density functional theory (DFT) calculations are performed within the projector augmented wave (PAW) method [38] and the Perdew-Burke-Ernzerhof (PBE) functional [39], as implemented in Vienna *Ab initio* Simulation Package (VASP) [40]. The kinetic-energy cutoff for the plane-wave basis is set to 520 eV and the force on each atom is less than 1×10^{-3} eV Å^{-1} to obtain a converged total energy. We apply the CE method established in alloy theory [35] to explore the $LaNiO_2H_\delta$ system. To search for intermediate ground-state structures at different H concentrations, we have utilized the Alloy-Theoretic Automated Toolkit (ATAT) code [41] and all atoms and lattice vectors are fully relaxed. ATAT randomly generates almost all possible 780 nonequivalent structures with each unit cell containing a maximum of 36 atoms, of which the formation energies (E_f) of 91 structures are calculated at the DFT level and subsequently used in the fitting process. The cross-validation score is set to 0.01 eV, which ensures the convergence of the CE fit in the calculation.

In addition, the DFT + *U* method is adopted [42] in all calculations, and *U* on Ni 3*d* is set to 5 eV unless specified, in agreement with previous reports [43]. For calculations exploring intermediate ground-state structures, spin-polarized calculation is not utilized. For the magnetic calculations at each H concentration ($\delta = 0$, 0.33, 0.5, 0.67, 0.83, 1), spin-polarized calculation is employed based on the nonmagnetic structures and supercells are used to accommodate possible magnetic configurations, and three possible spin configurations are calculated in each H concentration, i.e., ferromagnetic (FM), *C*-type antiferromagnetic (AFM-*C*, antiferromagnetic arrangement for in-plane Ni, and ferromagnetic arrangement for out of plane Ni), and AFM-*G* (both in-plane and out-of-plane Ni are antiferromagnetic arrangements). To compare the effect of inserted H atoms on electronic structures, all band structures calculated using the supercells are unfolded to the unit cell of $LaNiO_2$. The band unfolding is done by projecting supercell wave functions onto the primitive cell wave functions to determine the weights of primitive cell wave functions, enabling the calculation of the effective band structure for doped systems [44–46].

III. RESULTS AND DISCUSSION

A. Intermediate ground-state structures of $LaNiO_2H_\delta$

To explore the intermediate ground-state structures at various δ, we treat $LaNiO_2H_\delta$ as an alloy system and employ the CE method [35,41]. The basic idea of CE is to expand the energy of $LaNiO_2H_\delta$ into energetic contributions of cluster configurations based on a generalized (single atoms, pairs, triples, etc.) Ising Hamiltonian:

$$E_{(\sigma)} = J_0 + \sum_i J_i \hat{s}_i(\sigma) + \sum_{i<j} J_{ij} \hat{s}_i(\sigma)\hat{s}_j(\sigma) + \sum_{i<j<k} J_{ijk} \hat{s}_i(\sigma)\hat{s}_j(\sigma)\hat{s}_k(\sigma) + \dots . \quad (1)$$

The indexes *i*, *j*, and *k* run over all occupation positions, and $S_m(\sigma)$ takes on a value of either +1 or −1, indicating an occupied H and empty site, respectively. By employing the CE method, the energy $E_{(\sigma)}$ of any $LaNiO_2H_\delta$ alloy can be calculated by selecting a suitable value of J_α, which can be fitted from the DFT-calculated total energy of related structures [47].

The E_f of $LaNiO_2H_\delta$ is defined as

$$E_f = E[LaNiO_2H_\delta] - (1-\delta)E(LaNiO_2) - \delta E(LaNiO_2H), \quad (2)$$

where $E(LaNiO_2)$ and $E(LaNiO_2H)$ represent the energy of the $LaNiO_2$ and $LaNiO_2H$, respectively. The resulting convex hull diagram is shown in Fig. 1(a). The structures on the convex hull [red line in Fig. 1(a)] represent thermodynamically stable structures, while those above the convex hull correspond to metastable structures. Four intermediate ground states are determined with $\delta = 0.33$, 0.5, 0.67, and 0.83 where the corresponding structures are given in Figs. 1(b)–1(g), i.e., $LaNiO_2$ (D_{4h} symmetry), $LaNiO_2H_{0.33}$ (C_s symmetry), $LaNiO_2H_{0.5}$ (C_s symmetry), $LaNiO_2H_{0.67}$ (D_{2h} symmetry), $LaNiO_2H_{0.83}$ (C_{2h} symmetry), and $LaNiO_2H$ (D_{4h} symmetry). The corresponding lattice parameters are shown in Table I.

TABLE I. Structure parameters (lattice constant and angle) of the ground-state structures of $LaNiO_2H_\delta$ at $\delta = 0$, 0.33, 0.5, 0.67, 0.83, and 1.

δ	0	0.33	0.5	0.67	0.83	1
a(Å)	3.905	10.966	10.983	8.681	10.965	3.905
b(Å)	3.905	8.619	8.687	8.681	8.700	3.905
c(Å)	3.450	3.461	3.460	3.469	3.478	3.450
α(°)	90	90	90	90	90	90
β(°)	90	90	90	90	90	90
γ(°)	90	107.523	108.452	143.196	108.433	90

As shown in Fig. 1, we find that the insertion H located at the position of the apical oxygen vacancy site has the lowest energy. Interestingly, the H atoms in these four intermediate ground states show two universal features: (1) Along the out-of-plane direction, H atoms occupy the apical oxygen vacancies and form ordered H-Ni-H chains with strongly bonded Ni-3d_{z^2} orbital, consistent with previous studies [30–32]. We note that the formation of an ordered H-Ni-H chain is not caused by periodic boundary conditions, but is the consequence in terms of total energy. The formation of H-Ni-H chains is independent of the δ. (2) Along the in-plane direction, H atoms form different patterns. As shown in the lower panel of Figs. 1(c)–1(f), when $\delta = 0.33$, H atoms prefer a diagonal arrangement; when $\delta > 0.33$, H atoms are not diagonally arranged. Overall, our study indicates that H could form ordered states in $LaNiO_2$, instead of a random distribution. For an arbitrary δ, ideally, $LaNiO_2H_\delta$ may separate into a linear combination of its neighboring intermediate ground states.

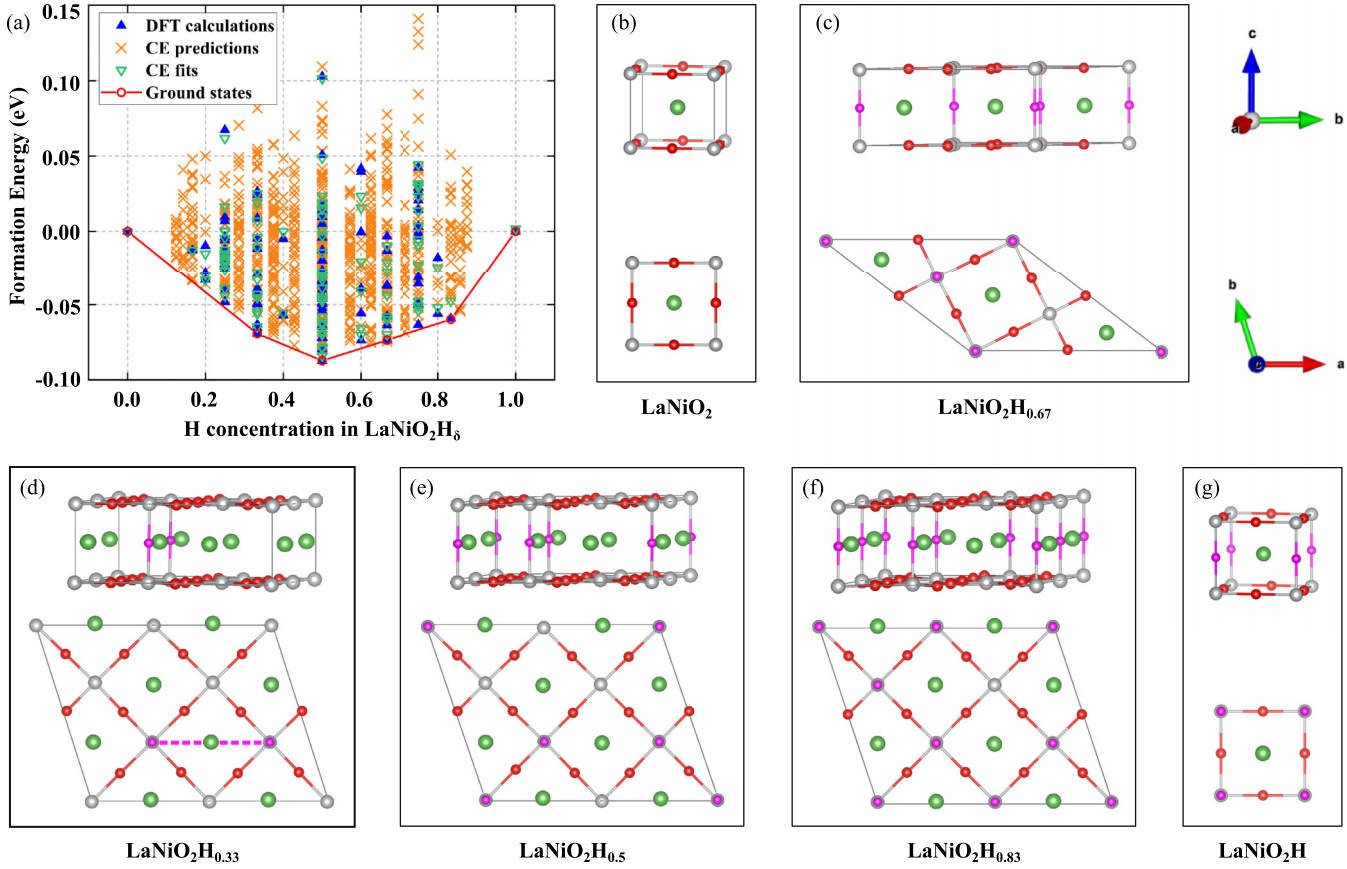

FIG. 1. Geometric structures of $LaNiO_2H_\delta$. (a) The calculated E_f with the corresponding CE fits as a function of H concentration δ. Panels (b)–(g) are ground-state structures at $\delta = 0$, 0.67, 0.33, 0.5, 0.83, and 1, respectively. The upper and lower panels correspond to the side and top views, respectively. The gray-solid line represents the primitive cell. The green, gray, red, and pink balls represent lanthanum (La), nickel (Ni), oxygen (O), and hydrogen (H) atoms, respectively. The pink dashed line represents a diagonal site.

B. Electronic structures of $LaNiO_2H_\delta$

To further investigate the evolution of electronic properties with δ, we draw the band structures and density of states (DOS) for these intermediate ground states with five major orbitals projections [La-5d_{z^2}, La-5d_{xy}, Ni-3d_{z^2}, Ni-3$d_{x^2-y^2}$, and interstitial s (IIs) orbital]. As shown in Fig. 2, except for $LaNiO_2H$, all structures have clear IIs states located at the apical oxygen vacancy [8,10,30]. With increasing δ, the intensity of this IIs state is reduced and finally annihilated while its position moves towards higher energy. Interestingly, the band structure along the *Z-R-A-Z* line and DOS show important features of the evolution of 3d orbitals: (i) the band dispersion of 3$d_{x^2-y^2}$ is hardly changed, while the energy level shifts slightly downward with increasing δ, and (ii) the band dispersion of 3d_{z^2} is changed greatly and the energy level moves close to the Fermi level (E_F). On the other hand, the band dispersion and orbital occupation of La 5d orbitals, with a small proportion around E_F, are barely changed.

In addition, the insertion of H leads to two different local environments of Ni. One Ni is at the face center of the NiO_4 square (denoted as Ni1), and the other is at the body center of the NiO_4H_2 octahedron (denoted as Ni2). The DOS for these two Ni atoms is drawn separately, showing different 3d orbitals filling. For Ni1, 3d_{z^2} is almost fully occupied, while 3$d_{x^2-y^2}$ is half filled. For Ni2, because of the strong bond with H 1s orbital, 3d_{z^2} is pushed up towards E_F. Meanwhile, the occupation of 3$d_{x^2-y^2}$ is increased in Ni2 compared with Ni1. For any intermediate ground-state structure, the DOS of 3d in the NiO_4 environment is similar to that in $LaNiO_2$ and 3d orbitals in the NiO_4H_2 environment are similar to that in $LaNiO_2H$, indicating the relatively local effect caused by the H insertion.

To qualitatively evaluate the filling variation of 3d orbital with δ, we integrate the DOS of total Ni-3d, 3$d_{x^2-y^2}$, and 3d_{z^2} orbitals under E_F, respectively. For the total 3d, as shown in Fig. 3(a), in $LaNiO_2$ the total 3d filling is 8.82 e and the corresponding valence of Ni is $+1.18\,e$, which is very close to the d^9 configuration and in agreement with previous DFT or dynamical mean-field theory (DMFT) studies [48,49]. With an increasing δ, the 3d filling decreases slightly and the orbital filling is decreased to 8.67 e in $LaNiO_2H$. This may be due to both the hole doping effect induced by H and the compensation effect of holes to IIs electrons [30]. For the 3$d_{x^2-y^2}$ orbital, as shown in Fig. 3(b), the orbital filling of Ni2 is increased by $\sim$0.3 e compared with Ni1 under different δ. For the 3d_{z^2} orbital, strong bonding is formed between the symmetry-matched Ni 3d_{z^2} and H 1s orbitals at the Ni2 site, causing the antibonding states pushed to higher energy and close to the E_F while the bonding states are down to an even lower energy level. Therefore, it is expected that the orbital

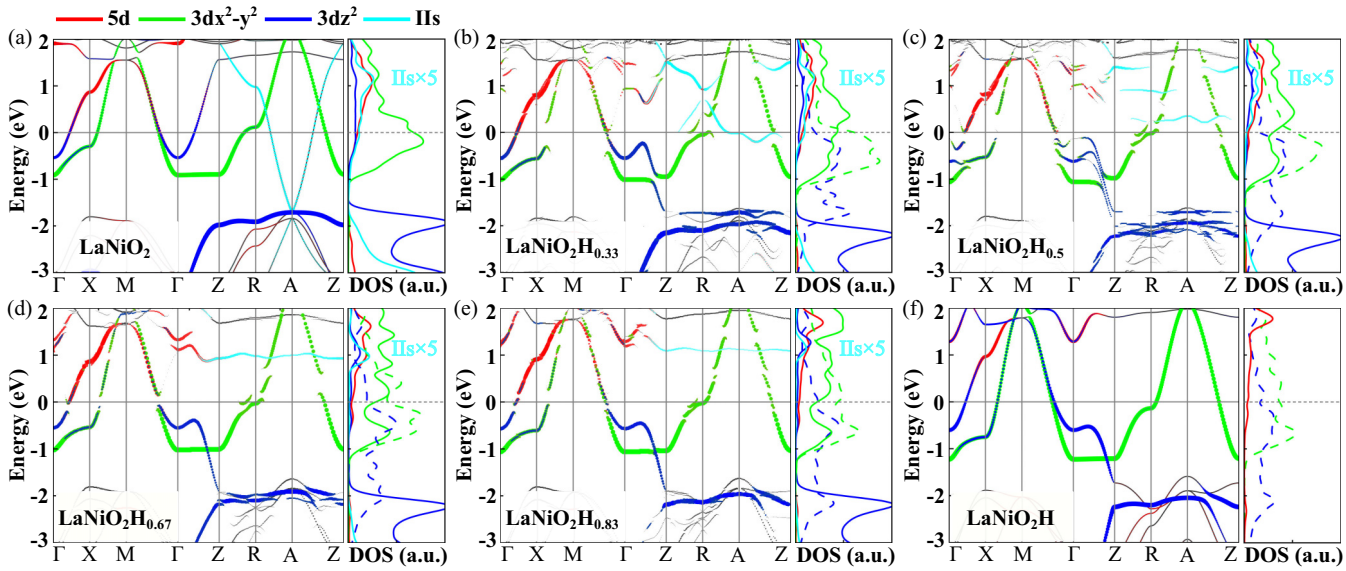

FIG. 2. Unfolded band structures and density of states (DOS) with orbital projections for $LaNiO_2H_\delta$ ($\delta = 0, 0.33, 0.5, 0.67, 0.83, 1$). The solid (dashed) lines in DOS are for the $3d$ orbitals in the NiO_4 (NiO_4H_2) environment. The DOS of IIs is enlarged by five times for the eyes. The E_F is set to zero.

filling of $3d_{z^2}$ at Ni2 site is smaller than that at Ni1 site, opposite to $3d_{x^2-y^2}$. Indeed, as shown in Fig. 3(c), the $3d_{z^2}$ filling of Ni2 is reduced by $\sim 0.2\,e$ compared to Ni1. This reduction is also identified from the band structures and DOS in Fig. 2: the projection of $3d_{z^2}$ around E_F increases more as δ increases. Therefore, considering the two opposite trends of $3d_{z^2}$ and $3d_{x^2-y^2}$ filling at Ni1 and Ni2 sites, the total $3d$ filling is less sensitive to δ in NiO_4 and NiO_4H_2 environments ($\sim 0.1\,e$), as shown in Fig. 3(a). That is, the insertion of H mainly reduces the occupation of the IIs orbital, leaving the occupation of the $3d$ orbitals hardly changed.

In addition, to better describe the electronic structures of transition metal oxides, electron-electron interaction is always taken into account by the Hubbard U formula. In infinite-layer nickelates, the value of U for Ni is set to 3–6 eV in DFT calculations [13,17,29,50]. To demonstrate that the electronic structures with different δ are insensitive to U, the band structure and DOS of $LaNiO_2$, $LaNiO_2H_{0.5}$, and $LaNiO_2H$ are also calculated with $U = 3$ eV, as shown in Fig. 4.

The electronic structures of $U = 3$ and 5 eV are thoroughly compared (Figs. 2 and 4). First, the bands with $U = 3$ eV shift slightly upward more than $U = 5$ eV, and the van Hove singularity with $U = 3$ eV is closer to E_F at the R point. Second, with $U = 3$ eV, the electronic pocket at the Γ point becomes smaller as a result of slight difference in Coulomb repulsion caused by U. Furthermore, despite different U, the evolution of orbital occupation and DOS with δ is consistent. Therefore, qualitatively our main conclusions are not influenced by the variation of U.

C. Magnetic properties of $LaNiO_2H_\delta$

Despite lacking long-range magnetic order [51,52], recent experiments have revealed short-range antiferromagnetic interactions in $RNiO_2$ [16,26]. So far, theoretical research of magnetic interaction behaviors [14,17,19,21,24,53–56] has focused on $RNiO_2$ systems without H doping while whether

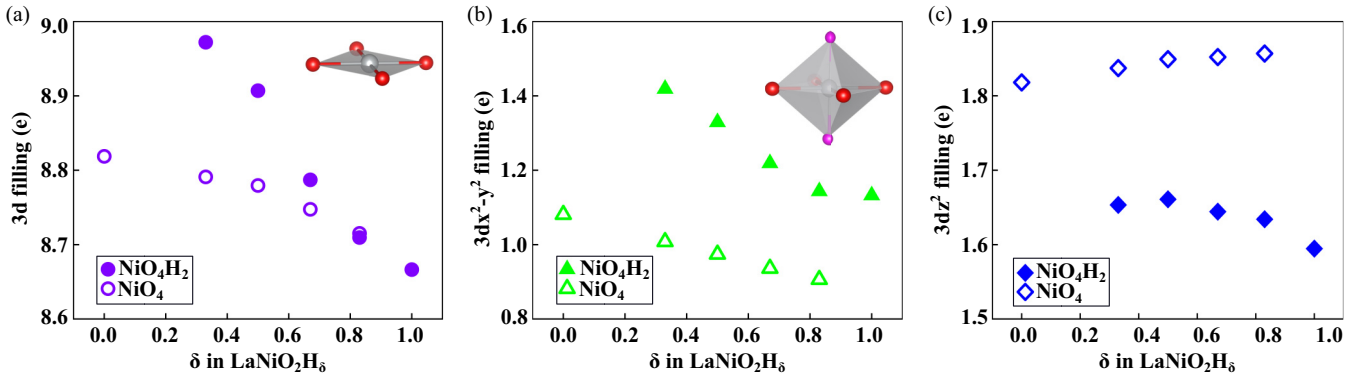

FIG. 3. Orbital fillings as a function of H concentration δ in $LaNiO_2H_\delta$. (a)–(c) Orbital fillings of total $3d$, $3d_{x^2-y^2}$, and $3d_{z^2}$ orbitals. Open and filled symbols represent the orbital fillings of Ni in Ni1 (NiO_4 environment) and Ni2 (NiO_4H_2 environment), respectively. The inset structures in (a) and (b) correspond to the local environments of Ni in Ni1 and Ni2, respectively.

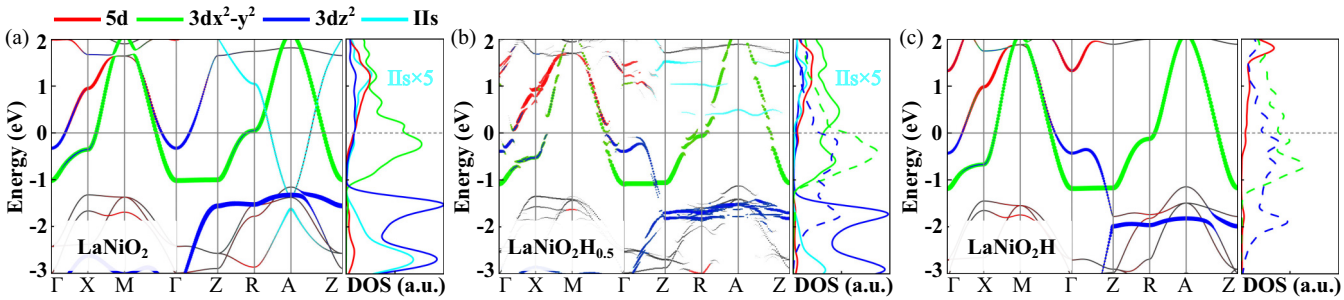

FIG. 4. Electronic structure of $LaNiO_2H_\delta$ with Hubbard $U = 3$ eV. (a)–(c) Unfolded band structures and DOS with orbital projections for $LaNiO_2$, $LaNiO_2H_{0.5}$, and $LaNiO_2H$. The solid (dashed) lines in DOS are for the $3d$ orbitals in the NiO_4 (NiO_4H_2) environment. The DOS of IIs is enlarged by five times for the eyes. The E_F is set to zero.

the magnetic interactions will be influenced by H is still an open question.

For each δ, to explore the magnetic properties in $LaNiO_2H_\delta$ we have calculated the total energy of nonmagnetic (NM), FM, AFM-C, and AFM-G states, and the results are shown in Fig. 5(a), where the energy of the AFM-G configuration is set to zero as a reference. For $LaNiO_2$, the energies of different magnetic orders are comparable. The energies of AFM-G and FM configurations are pretty close, and both are only ~3 meV/Ni higher than the AFM-C configuration, indicating that AFM-C is the ground state, consistent with the previous theoretical study [57]. Interestingly, with δ increases, the energy differences between different magnetic configurations also increase, while the magnetic ground-state configuration is stabilized as the AFM-G state. Therefore, H plays an important role to distinguish the different magnetic ground-state configurations. For example, with $\delta = 0.33$, AFM-G is ~60 meV/Ni lower than AFM-C and FM. As δ increases from 0.5 to 1, the AFM-G is more stable, whereas the energy of AFM-C becomes much lower than FM, indicating stronger antiferromagnetic interaction with increasing δ. Figure 5(b) shows the total DOS of three magnetic configurations with $\delta = 0$, 0.5, and 1, respectively, as an illustration of the effect of H doping on magnetic properties. For FM, the systems are all metal despite different δ. For AFM-C and AFM-G, there is a metal-insulator phase transition under H doping. $LaNiO_2$ is a metal phase, which transforms into an insulator phase in $LaNiO_2H$. Besides, the band gap of the H-doped AFM-G is more prominent than that of the AFM-C.

The above discussion shows that, in $LaNiO_2H_\delta$, as H concentration increases, AFM-G is the dominant magnetic ground state. Therefore, focusing on the metal-insulator transition (under the DFT + U level calculations) in the AFM-G state, we have analyzed the evolution of band structures and DOS with increasing δ, as shown in Fig. 6. First of all, the orbitals near E_F are mainly IIs, $3d_{x^2-y^2}$ and $3d_{z^2}$ in $LaNiO_2$, as shown in Fig. 6(a). With the increase of δ, the IIs orbital is gradually annihilated and the coupling between IIs and $3d_{z^2}$ is weakened, leading to the opening of the band gap. In addition, the band gap becomes larger with increasing δ (0, 0.51, 0.50, 0.75, 0.71, and 1.75 eV for $\delta = 0$, 0.33, 0.5, 0.67, 0.83, and 1, respectively) and the band gap of $LaNiO_2H$ is the largest, as detailed in Figs. 6(a)–6(f). Furthermore, the occupation of the $3d_{z^2}$ orbital decreases with increasing δ, similar to the

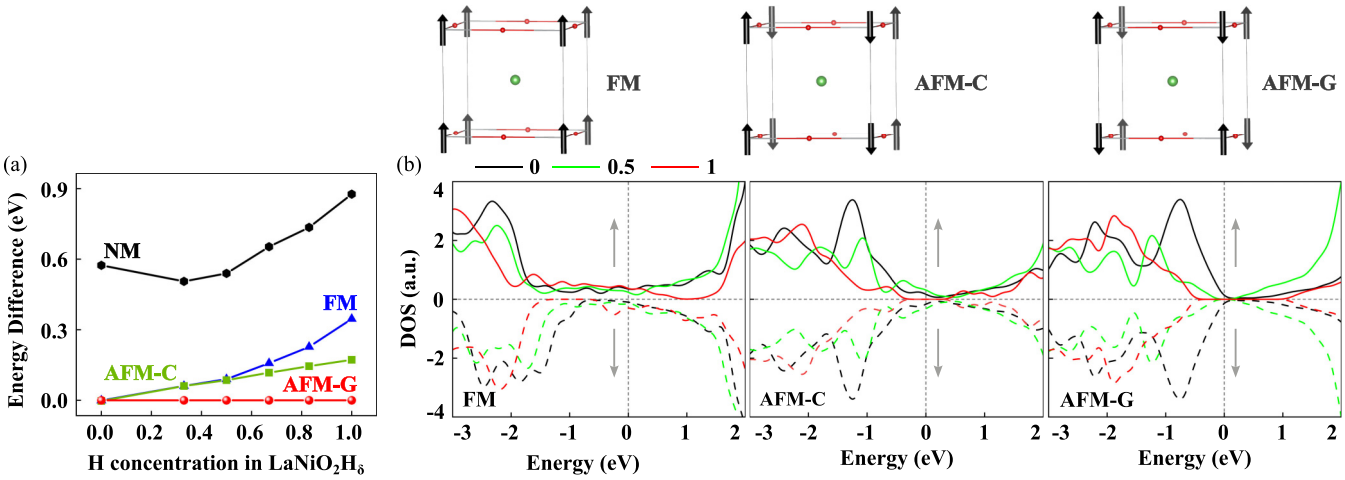

FIG. 5. The energy difference and total DOS of three spin configurations in $LaNiO_2H_\delta$. (a) The energy difference between NM, FM, AFM-C, and AFM-G as a function of H concentration in $LaNiO_2H_\delta$. (b) The total DOS of FM, AFM-C, and AFM-G in $LaNiO_2$, $LaNiO_2H_{0.5}$, and $LaNiO_2H$. The black, green, and red lines represent H concentrations of 0, 0.5, and 1, respectively. The solid and dashed lines represent the majority and minority spin, respectively, as indicated by the direction of the gray arrow. The E_F is set to zero. Insets are schematics of three magnetic configurations: FM, AFM-C, and AFM-G.

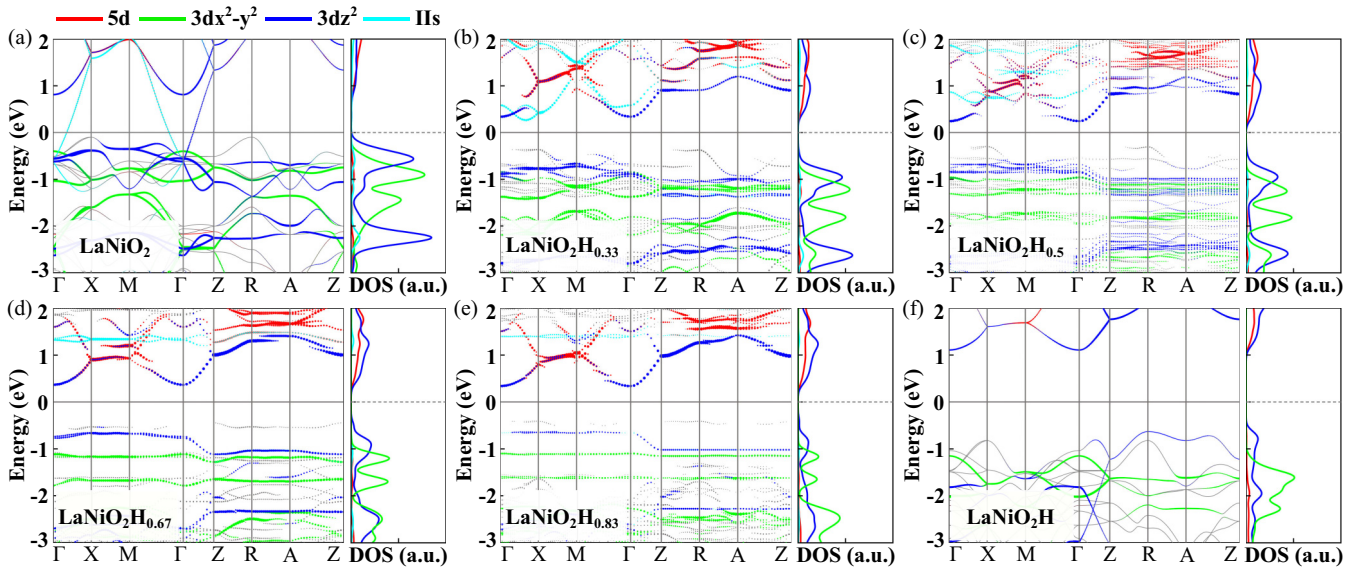

FIG. 6. The electronic structures under AFM-G configuration. (a)–(f) Unfolded band structures and DOS with orbital projections for $LaNiO_2$, $LaNiO_2H_{0.33}$, $LaNiO_2H_{0.5}$, $LaNiO_2H_{0.67}$, $LaNiO_2H_{0.83}$, and $LaNiO_2H$. Only spin-up projected orbitals are shown. The E_F is set to zero.

NM case. This is due to the repulsive interaction between the energy level of $3d_{z^2}$ and H-1s; the bonding like $3d_{z^2}$ orbital is pushed away from the E_F and the antibonding like $3d_{z^2}$ orbital is pushed above the E_F. Additionally, the occupation of $3d_{x^2-y^2}$ in the AFM-G state is completely different from that in the NM state: $3d_{x^2-y^2}$ is almost fully occupied below the E_F in the AFM-G state, while it is partially occupied in the NM state. Besides, the occupation of La 5d orbital is insensitive to H. Overall, H doping leads to a metal-to-insulator transition with a critical concentration δ of 0.33 and approaches a d^9 insulating state.

IV. CONCLUSION

Using the first-principles calculations in the $LaNiO_2H_\delta$ system, we find that H always forms an ordered H-Ni-H chain along the out-of-plane direction due to the strong bonding of Ni-d_{z^2} and H-1s states. In addition, H doping can adjust the band ratio of $3d_{z^2}$ and $3d_{x^2-y^2}$ and tune the orbital polarization, which may be one reason for the observed superconductivity in a certain H concentration in the experiment. Regarding magnetism properties, there is competition between different magnetic orders. This system is eventually stabilized to the AFM-G ground state with increasing H concentration, with the presence of strong antiferromagnetic interactions. As the H concentration increases, a metal-to-insulator transition occurs in the AFM state. These results suggest that H may play an important role in the fundamental electronic structure of $LaNiO_2H_\delta$, and our work may also potentially contribute to the understanding of infinite-layer nickelates superconductivity.

ACKNOWLEDGMENTS

This work was supported by the National Key Research and Development of China (Grant No. 2022YFA1402401), NSFC (Grant No. 12088101), and NSAF (Grant No. U2230402). Computations were done at the Tianhe-JK supercomputer at CSRC.

[1] D. Li, K. Lee, B. Y. Wang, M. Osada, S. Crossley, H. R. Lee, Y. Cui, Y. Hikita, and H. Y. Hwang, Superconductivity in an infinite-layer nickelate, Nature (London) **572**, 624 (2019).

[2] S. Zeng, C. S. Tang, X. Yin, C. Li, M. Li, Z. Huang, J. Hu, W. Liu, G. J. Omar, H. Jani *et al.*, Phase diagram and superconducting dome of infinite-layer $Nd_{1-x}Sr_xNiO_2$ thin films, Phys. Rev. Lett. **125**, 147003 (2020).

[3] Q. Gu, Y. Li, S. Wan, H. Li, W. Guo, H. Yang, Q. Li, X. Zhu, X. Pan, Y. Nie *et al.*, Single particle tunneling spectrum of superconducting $Nd_{1-X}Sr_xNiO_2$ thin films, Nat. Commun. **11**, 6027 (2020).

[4] M. Osada, B. Y. Wang, B. H. Goodge, K. Lee, H. Yoon, K. Sakuma, D. Li, M. Miura, L. F. Kourkoutis, and H. Y. Hwang, A superconducting praseodymium nickelate with infinite layer structure, Nano Lett. **20**, 5735 (2020).

[5] M. Osada, B. Y. Wang, K. Lee, D. Li, and H. Y. Hwang, Phase diagram of infinite layer praseodymium nickelate $Pr_{1-x}Sr_xNiO_2$ thin films, Phys. Rev. Mater. **4**, 121801 (2020).

[6] M. Osada, B. Y. Wang, B. H. Goodge, S. P. Harvey, K. Lee, D. Li, L. F. Kourkoutis, and H. Y. Hwang, Nickelate superconductivity without rare-earth magnetism: (La, Sr) NiO_2, Adv. Mater. **33**, 2104083 (2021).

[7] G. A. Pan, D. F. Segedin, H. LaBollita, Q. Song, E. M. Nica, B. H. Goodge, A. T. Pierce, S. Doyle, S. Novakov, D. C. Carrizales *et al.*, Superconductivity in a quintuple-layer square-planar nickelate, Nat. Mater. **21**, 160 (2022).

[8] Y. Nomura, M. Hirayama, T. Tadano, Y. Yoshimoto, K. Nakamura, and R. Arita, Formation of a two-dimensional single-component correlated electron system and band engineering in the nickelate superconductor $NdNiO_2$, Phys. Rev. B **100**, 205138 (2019).

[9] A. S. Botana and M. R. Norman, Similarities and differences between $LaNiO_2$ and $CaCuO_2$ and implications for superconductivity, Phys. Rev. X **10**, 011024 (2020).

[10] Y. Gu, S. Zhu, X. Wang, J. Hu, and H. Chen, A substantial hybridization between correlated Ni-d orbital and itinerant electrons in infinite-layer nickelates, Commun. Phys. **3**, 84 (2020).

[11] H. Sakakibara, H. Usui, K. Suzuki, T. Kotani, H. Aoki, and K. Kuroki, Model construction and a possibility of cuprate like pairing in a New d^9 nickelate superconductor (Nd, Sr) NiO_2, Phys. Rev. Lett. **125**, 077003 (2020).

[12] F. Lechermann, Multiorbital processes rule the $Nd_{1-x}Sr_xNiO_2$ normal state, Phys. Rev. X **10**, 041002 (2020).

[13] M.-Y. Choi, K.-W. Lee, and W. E. Pickett, Role of $4f$ states in infinite-layer $NdNiO_2$, Phys. Rev. B **101**, 020503 (2020).

[14] V. M. Katukuri, N. A. Bogdanov, O. Weser, J. van den Brink, and A. Alavi, Electronic correlations and magnetic interactions in infinite-layer $NdNiO_2$, Phys. Rev. B **102**, 241112 (2020).

[15] M. Jiang, M. Berciu, and G. A. Sawatzky, Critical nature of the Ni spin state in doped $NdNiO_2$, Phys. Rev. Lett. **124**, 207004 (2020).

[16] H. Lu, M. Rossi, A. Nag, M. Osada, D. F. Li, K. Lee, B. Y. Wang, M. Garcia-Fernandez, S. Agrestini, Z. X. Shen *et al.*, Magnetic excitations in infinite-layer nickelates, Science **373**, 213 (2021).

[17] E. Been, W.-S. Lee, H. Y. Hwang, Y. Cui, J. Zaanen, T. Devereaux, B. Moritz, and C. Jia, Electronic structure trends across the rare-earth series in superconducting infinite-layer nickelates, Phys. Rev. X **11**, 011050 (2021).

[18] H. LaBollita and A. S. Botana, Electronic structure and magnetic properties of higher-order layered nickelates: $La_{n+1}Ni_nO_{2n+2}$ $La_{n+1}Ni_nO_{2n+2}$, Phys. Rev. B **104**, 035148 (2021).

[19] X. Wan, V. Ivanov, G. Resta, I. Leonov, and S. Y. Savrasov, Exchange interactions and sensitivity of the Ni two-hole spin state to Hund's coupling in doped $NdNiO_2$, Phys. Rev. B **103**, 075123 (2021).

[20] J. Q. Lin, P. V. Arribi, G. Fabbris, A. S. Botana, D. Meyers, H. Miao, Y. Shen, D. G. Mazzone, J. Feng, S. G. Chiuzbăian *et al.*, Strong superexchange in a $d^{9-\delta}$ nickelate revealed by resonant inelastic x-ray scattering, Phys. Rev. Lett. **126**, 087001 (2021).

[21] L.-H. Hu and C. Wu, Two-band model for magnetism and superconductivity in nickelates, Phys. Rev. Res. **1**, 032046 (2019).

[22] A. Kreisel, B. M. Andersen, A. T. Rømer, I. M. Eremin, and F. Lechermann, Superconducting instabilities in strongly correlated infinite-layer nickelates, Phys. Rev. Lett. **129**, 077002 (2022).

[23] P. Worm, L. Si, M. Kitatani, R. Arita, J. M. Tomczak, and K. Held, Correlations tune the electronic structure of pentalayer nickelates into the superconducting regime, Phys. Rev. Mater. **6**, L091801 (2022).

[24] D. Chen, P. Jiang, L. Si, Y. Lu, and Z. Zhong, Magnetism in doped infinite-layer $NdNiO_2$ studied by combined density functional theory and dynamical mean-field theory, Phys. Rev. B **106**, 045105 (2022).

[25] D. Zhao, Y. B. Zhou, Y. Fu, L. Wang, X. F. Zhou, H. Cheng, J. Li, D. W. Song, S. Li, B. L. Kang *et al.*, Intrinsic spin susceptibility and pseudogap-like behavior in infinite-layer $LaNiO_2$, Phys. Rev. Lett. **126**, 197001 (2021).

[26] Y. Cui, C. Li, Q. Li, X. Zhu, Z. Hu, Y. Yang, J. Zhang, R. Yu, H.-H. Wen, and W. Yu, NMR evidence of antiferromagnetic spin fluctuations in $Nd_{0.85}Sr_{0.15}NiO_2$, Chin. Phys. Lett. **38**, 067401 (2021).

[27] G. Krieger, L. Martinelli, S. Zeng, L. E. Chow, K. Kummer, R. Arpaia, M. M. Sala, N. B. Brookes, A. Ariando, N. Viart *et al.*, Charge and spin order dichotomy in $NdNiO_2$ driven by the capping layer, Phys. Rev. Lett. **129**, 027002 (2022).

[28] C. C. Tam, J. Choi, X. Ding, S. Agrestini, A. Nag, M. Wu, B. Huang, H. Luo, P. Gao, M. García-Fernández *et al.*, Charge density waves in infinite-layer $NdNiO_2$ nickelates, Nat. Mater. **21**, 1116 (2022).

[29] M. Hepting, D. Li, C. J. Jia, H. Lu, E. Paris, Y. Tseng, X. Feng, M. Osada, E. Been, Y. Hikita *et al.*, Electronic structure of the parent compound of superconducting infinite-layer nickelates, Nat. Mater. **19**, 381 (2020).

[30] X. Ding, C. C. Tam, X. Sui, Y. Zhao, M. Xu, J. Choi, H. Leng, J. Zhang, M. Wu, H. Xiao *et al.*, Critical role of hydrogen for superconductivity in nickelates, Nature (London) **615**, 50 (2023).

[31] L. Si, W. Xiao, J. Kaufmann, J. M. Tomczak, Y. Lu, Z. Zhong, and K. Held, Topotactic hydrogen in nickelate superconductors and akin infinite-layer oxides ABO_2, Phys. Rev. Lett. **124**, 166402 (2020).

[32] L. Si, P. Worm, D. Chen, and K. Held, Topotactic hydrogen forms chains in ABO_2 nickelate superconductors, Phys. Rev. B **107**, 165116 (2023).

[33] B. Huang, H. J. Xiang, and S.-H. Wei, Chemical functionalization of silicene: Spontaneous structural transition and exotic electronic properties, Phys. Rev. Lett. **111**, 145502 (2013).

[34] B. Huang, H.-X. Deng, H. Lee, M. Yoon, B. G. Sumpter, F. Liu, S. C. Smith, and S.-H. Wei, Exceptional optoelectronic properties of hydrogenated bilayer silicene, Phys. Rev. X **4**, 021029 (2014).

[35] L. G. Ferreira, S. H. Wei, and A. Zunger, First-principles calculation of alloy phase diagrams: The renormalized-interaction approach, Phys. Rev. B **40**, 3197 (1989).

[36] Y. Li, S. Du, Z.-Y. Weng, and Z. Liu, In-Plane ordering of oxygen vacancies in a High-T_c cuprate superconductor with compressed Cu-O octahedrons: An automated cluster expansion study, Phys. Rev. Mater. **4**, 044801 (2020).

[37] P. A. Korzhavyi, C. Ambrosch-Draxl, and B. Johansson, *Ab-initio* study of the vacancy ordering in $YBa_2Cu_3O_{7-x}$, J. Low Temp. Phys. **117**, 395 (1999).

[38] P. E. Blöchl, Projector augmented-wave method, Phys. Rev. B **50**, 17953 (1994).

[39] J. P. Perdew, K. Burke, and M. Ernzerhof, Generalized gradient approximation made simple, Phys. Rev. Lett. **77**, 3865 (1996).

[40] G. Kresse and J. Furthmüller, Efficient iterative schemes for *ab* initio total-energy calculations using a plane-wave basis set, Phys. Rev. B **54**, 11169 (1996).

[41] A. Van De Walle, M. Asta, and G. Ceder, The alloy theoretic automated toolkit: A user guide, Calphad **26**, 539 (2002).

[42] S. L. Dudarev, G. A. Botton, S. Y. Savrasov, C. J. Humphreys, and A. P. Sutton, Electron-Energy-Loss spectra and the

structural stability of nickel oxide: An LSDA + U study, Phys. Rev. B **57**, 1505 (1998).

[43] Z. Chen, M. Osada, D. Li, E. M. Been, S.-D. Chen, M. Hashimoto, D. Lu, S.-K. Mo, K. Lee, B. Y. Wang *et al.*, Electronic structure of superconducting nickelates probed by resonant photoemission spectroscopy, Matter **5**, 1806 (2022).

[44] V. Popescu and A. Zunger, Extracting E versus k effective band structure from supercell calculations on alloys and impurities, Phys. Rev. B **85**, 085201 (2012).

[45] P. V. C. Medeiros, S. Stafström, and J. Björk, Effects of extrinsic and intrinsic perturbations on the electronic structure of graphene: Retaining an effective primitive cell band structure by band unfolding, Phys. Rev. B **89**, 041407 (2014).

[46] W. Ku, T. Berlijn, and C.-C. Lee, Unfolding first-principles band structures, Phys. Rev. Lett. **104**, 216401 (2010).

[47] *Handbook of Materials Modeling*, edited by B. Huang and S.-H. Wei (Springer, Cham, 2020), p. 568.

[48] Z. Liu, C. Xu, C. Cao, W. Zhu, Z. F. Wang, and J. Yang, Doping dependence of electronic structure of infinite-layer $NdNiO_2$, Phys. Rev. B **103**, 045103 (2021).

[49] Y. Wang, C.-J. Kang, H. Miao, and G. Kotliar, Hund's Metal physics: From $SrNiO_2$ to $LaNiO_2$, Phys. Rev. B **102**, 161118 (2020).

[50] X. Liao, V. Singh, and H. Park, Oxygen vacancy induced site-selective mott transition in $LaNiO_3$, Phys. Rev. B **103**, 085110 (2021).

[51] B.-X. Wang, H. Zheng, E. Krivyakina, O. Chmaissem, P. P. Lopes, J. W. Lynn, L. C. Gallington, Y. Ren, S. Rosenkranz, J. F. Mitchell *et al.*, Synthesis and characterization of bulk $Nd_{1-x}Sr_xNiO_2$ and $Nd_{1-x}Sr_xNiO_3$, Phys. Rev. Mater. **4**, 084409 (2020).

[52] M. A. Hayward, M. A. Green, M. J. Rosseinsky, and J. Sloan, Sodium hydride as a powerful reducing agent for topotactic oxide deintercalation: Synthesis and characterization of the Nickel (I) Oxide $LaNiO_2$, J. Am. Chem. Soc. **121**, 8843 (1999).

[53] M.-Y. Choi, W. E. Pickett, and K.-W. Lee, Fluctuation-Frustrated flat band instabilities in $NdNiO_2$, Phys. Rev. Res. **2**, 033445 (2020).

[54] Z. Liu, Z. Ren, W. Zhu, Z. Wang, and J. Yang, Electronic and magnetic structure of infinite-layer $NdNiO_2$: Trace of antiferromagnetic metal, npj Quantum Mater. **5**, 31 (2020).

[55] G.-M. Zhang, Y. Yang, and F.-C. Zhang, Self-Doped mott insulator for parent compounds of nickelate superconductors, Phys. Rev. B **101**, 020501 (2020).

[56] S. Ryee, H. Yoon, T. J. Kim, M. Y. Jeong, and M. J. Han, Induced magnetic two-dimensionality by hole doping in the superconducting infinite-layer nickelate $Nd_{1-x}Sr_xNiO_2$, Phys. Rev. B **101**, 064513 (2020).

[57] J. Kapeghian and A. S. Botana, Electronic structure and magnetism in infinite-layer nickelates $RNiO_2$ (R = La − Lu), Phys. Rev. B **102**, 205130 (2020).